INFLUENCE OF Fe^{3+} AND Eu^{3+} DOPING ON STRUCTURAL, OPTICAL AND MAGNETIC PROPERTIES OF ZnO NANOPARTICLES

P. T. POOJITHA[a*], V. K. MADHU SMITHA[a], S. BABU[b], M. KUMAR[c], S.V. PRABHAKAR VATTIKUTI[d*]

[a]*Department of Physics, Siddartha Educational Academy Group of Institutions, Tirupati – 517502, India*
[b]*Department of Physics, Sri Venkateswara University, Tirupati-517 50, India*
[c]*Department of Electronic Engineering, Yeungnam University, Gyeongsan 38541, South Korea*
[d]*School of Mechanical Engineering, Yeungnam University, Gyeongsan 38541, South Korea*

Ethylenediaminetetraacetic acid (EDTA) passivated pristine, Fe^{3+} and Eu^{3+} doped ZnO nanoparticles (NPs) have been synthesized by chemical-refluxing technique at 100 ^{o}C. The X-ray diffraction studies of all the prepared NPs display the formation of hexagonal phase with the absence of further impurities. Low resolution transmission electron microscopy analysis depicts the formation of polydispersed NPs with the size of ~25 nm. The three optical modes of all the NPs are in good consensus with the characteristic Raman peaks of standard hexagonal ZnO. Diffuse Reflectance Spectroscopy showed both blue shift and red shift of the Fe^{3+} and Eu^{3+} doped ZnO NPs compared to that of pristine ZnO, which further attested the incorporation of Fe^{3+} and Eu^{3+} into the ZnO matrix as a substitute. It is found that the magnetic properties of the synthesized NPs showed diamagnetism for pristine and paramagnetism for both Fe^{3+} and Eu^{3+} doped ZnO.

1. Introduction

In the past few years, diluted magnetic semiconductors (DMS) have been extensively studied in view of their unique properties and are II-VI, II-V, IV-VI or III-V based semiconductor compounds in which the cations are randomly replaced by dopant magnetic ions like transition or rare-earth metals. The great interest in studying these materials is stimulated by their unique electronic, magnetic and magneto-optical properties [1, 2]. It is believed that, the structure as well as semiconductor properties such as the lattice parameters and band gap can be varied in a controlled fashion by changing the composition. In addition, the existence of exchange interaction between band electrons and magnetic ions induces many physical effects, such as magnetic polaron [3], large Faraday rotation [4] and the giant negative magnetoresistance [5]. The magnetic properties and the exchange interaction with band electrons distinguish these materials from other semiconductors. Due to this reason, the diluted magnetic semiconductors are also known as semimagnetic semiconductors and the possibility of using electron spins in spintronic devices has attracted growing interest in DMS. Recently, the interest significantly increased on ZnO based diluted magnetic semiconductors owing to their unique electrical, magnetic, mechanical, and optical properties, leading to many potential applications [6-10]. Especially in nano form, ZnO has been promising material for supporting the room temperature ferromagnetism [6, 7, 10]. Although, the origin and mechanism of the ferromagnetism (FM) remain disputable. Various chemical routes are available for the fabrication of ZnO nanoparticles such as co-precipitation, hydrothermal, sol-

---

*Corresponding author: vsvprabu@gmail.com

gel, spin coating co-precipitation, etc. Among them, chemical refluxing is very economical and very easy to fabricate the best quality samples.

In this paper, we demonstrated the structural, optical and magnetic properties of Pristine, Fe^{3+} and Eu^{3+} doped ZnO nanoparticles via chemical refluxing technique at 100 °C using EDTA as a surfactant.

2. Experimental

Pristine and 3 at.% of Fe^{3+} and Eu^{3+} doped ZnO NPs were synthesized by chemical-refluxing technique at 100 °C using EDTA as a surfactant. All of the chemical reagent used in this work, including zinc acetate, ferric chloride, europium nitrate, and sodium hydroxide, is AR grade. 0.2 M zinc acetate and pertinent amounts of ferric chloride/ europium nitrate were mixed with 50 ml of Millipore water. After that, a sodium hydroxide solution was added drop by drop to the above mixture. Eventually, 0.1 g of EDTA was added to that solution as a surfactant and refluxed for 5 h at a temperature of 100 °C. The precipitate, containing iron and europium doped ZnO NPs, obtained was washed with absolute ethanol and was dried in an oven at 100 °C for 12 h.

The structural and phase purity were investigated by X-ray diffraction (Seifert 3003 TT X-ray diffractometer (λ =1.540 Å) with Cu-Kα radiation) and the system was operated at 40 KeV and 30 mA in a scan range of 20-70°. To determine the particle size of the synthesized samples (Model: Phillips, TECHNAI FE 12) was performed through a transmission electron microscope. Raman scattering experiments were carried out using a micro-Raman spectrometer (Horiba Jobin Yvon HR 800 UV confocal) at room temperature. To find the optical band gaps of the synthesized NPs were carried out by using diffuse reflectance spectroscopy (Model: Jasco V-670 double-beam spectrometer). The room temperature magnetic properties of the synthesized NPs were carried out using a vibrating sample magnetometer (Lakshore, 7410).

3. Results and discussion

3.1. Structural analysis

The representative X-ray diffraction patterns of the pristine, Fe^{3+} and Eu^{3+} doped ZnO NPs are shown in Fig. 1. The diffraction peaks of the pristine, Fe^{3+} and Eu^{3+} doped ZnO NPs located at the same positions with those of hexagonal ZnO (JCPDS: 36-1451). Additional reflections are not observed for all the samples within the detection limit of the XRD instrument, indicating that, there is no impurity phases presenting in the synthesized samples. Broad diffraction peaks of the samples stipulate the nanocrystalline nature.
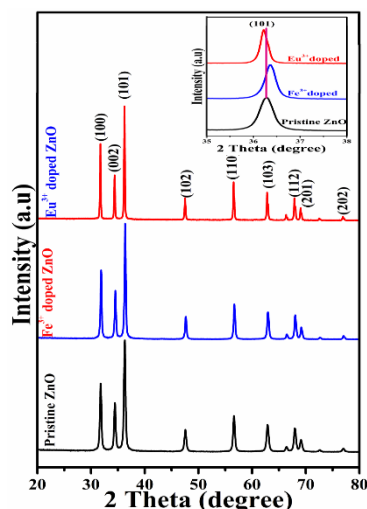

Fig. 1. XRD patterns and (inset) the magnified region of (101) peak of the (a) pristine,
(b) Fe^{3+} doped and (c) Eu^{3+} doped ZnO NPs

The peak position of the Iron doped sample slightly shifts towards higher 2θ value, which clearly results the smaller ionic radius of Fe^{3+} (0.645 Å) compared to that of Zinc (0.74 Å) in the ZnO and the peak positions of Eu^{3+} doped sample showed a trivial shift towards lower 2θ value, since, the ionic radius of Eu^{3+} (0.947 Å) was much bigger than that of Zinc (0.74 Å). These observations indicating that the successful incorporation of the dopant ions into the ZnO host lattice. The average crystallite size 'D' of the synthesized samples are evaluated according to the Debye–Scherrer equation, $D = 0.89\ \lambda\ /\ \beta\ Cos\ \theta$, where D is the average crystallite size of the particle, λ is the wavelength of the X-rays, β is the full width at half maximum intensity of the diffraction peak and θ is the diffraction angle. The assessed average crystallite size was found to be 22 ± 2 nm, 19 ± 0.7 and 24 ± 1.3 nm for pristine, Fe^{3+} and Eu^{3+} doped ZnO samples, respectively.

3.2. TEM analysis

Fig. 2 (a)-(c) shows the pristine, Fe^{3+} and Eu^{3+} doped ZnO NPs. It can see that the formation of polydisperse nanoparticles with closely hexagonal shape and irregular size distribution. Polydispersity is the regular hurdle in the NPs. Since they have a higher excessive relative number of surface atoms and relative surface area.
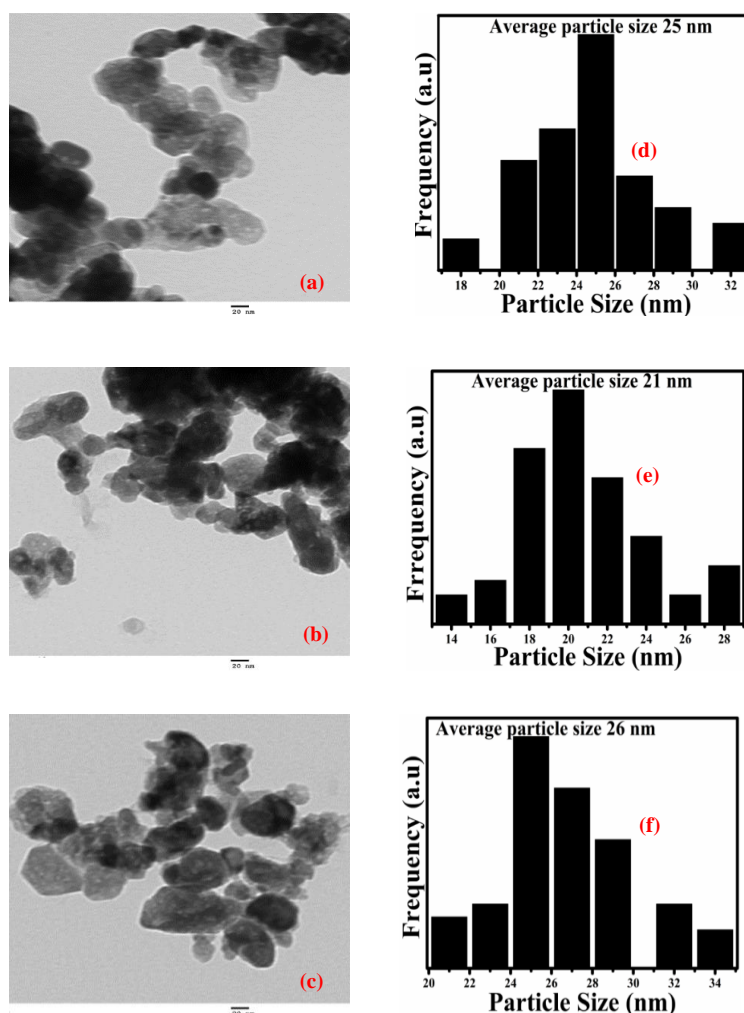

Fig. 2. TEM images of (a) pristine, (b) Fe^{3+} doped and (c) Eu^{3+} doped ZnO NPs and size distributions of (d) pristine, (e) Fe^{3+} and (f) Eu^{3+} doped ZnO NPs

The atoms have unsaturated coordination and each atom have vacant coordinate sites. They try to get the bonds, this results the agglomeration in NPs. The inset of Fig. 2 (d)-(f) displays the volume average size distribution histogram. The assessed average diameter of the synthesized nanoparticles were 25, 20 and 26 nm for pristine, Fe^{3+} doped and Eu^{3+} doped ZnO NPs, respectively. The particle size is analyzed and calculated by using the Image J software.

3.3. Raman analysis

Additional information on the structure of the synthesized NPs is also analyzed through Raman spectroscopy. Fig. 3 depicts the micro-Raman spectra of the Pristine, Fe^{3+} and Eu^{3+} doped ZnO at the range of 100 – 800 cm^{-1} at room temperature. The optical mode around 336 cm^{-1} is assigned to a second order spectral feature emanated from the zone boundary phonons of $2\text{-}E_2$ (M) to zinc oxide [11], the optical mode around 436 cm^{-1} can be assigned to the nonpolar E_2 (high) optical mode of zinc oxide [12] and the final optical mode around 580 cm^{-1} could be assigned as longitudinal optical (LO) mode (A_1 (LO)). The appearance of optical mode E_2 (high) in all the samples conforming the hexagonal structure of ZnO, which is in good agreement with the X-ray diffraction studies. The optical modes of the Fe^{3+} and Eu^{3+} doped ZnO slightly shifted to lower frequencies compared to the pristine sample, which may be due to the successful incorporation of Zn by dopant ions in the doped ZnO lattice. No other peaks related to other secondary phases are noticed in the Fe^{3+} and Eu^{3+} doped ZnO NPs.
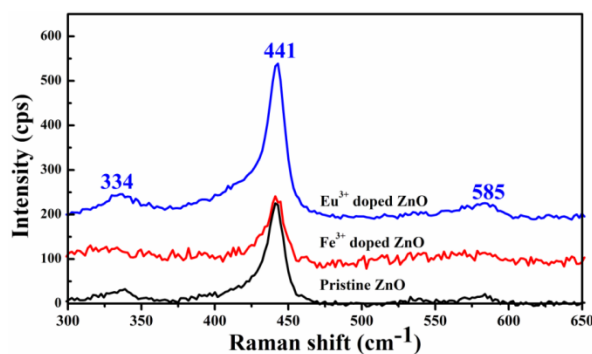

Fig. 3 Raman spectra of pristine, Fe^{3+} and Eu^{3+} doped ZnO NPs

3.4. DRS analysis

To know the band gaps of the pristine, Fe^{3+} and Eu^{3+} doped ZnO NPs, diffuse reflectance spectroscopy measurements were carried out. Fig. 4 illustrated the DRS spectra of pristine, Fe^{3+} and Eu^{3+} doped ZnO NPs. From this figure, we recognized the blue shift in the Fe^{3+} doped sample and red shift in the Eu^{3+} doped ZnO samples. The blue shift of the Fe^{3+} doped sample, indicating an increase in the bandgap compares to pristine ZnO. The red shift of the Eu^{3+} doped ZnO is a consequence of the *sp-f* spin exchange interaction among the localized *d* electrons and band electrons of the Eu^{3+} ions. The assessed band gaps are found to be 3.6, 3.8 and 3.50 eV for pristine, Fe^{3+} and Eu^{3+} doped ZnO NPs (Fig. 5).
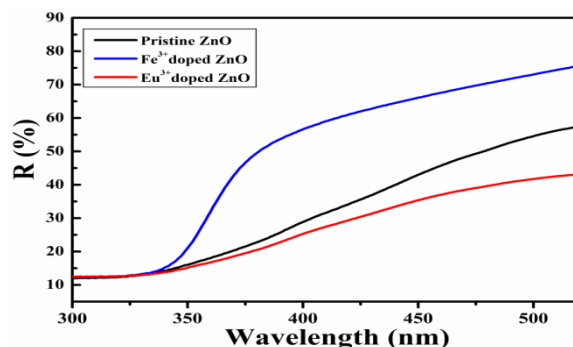

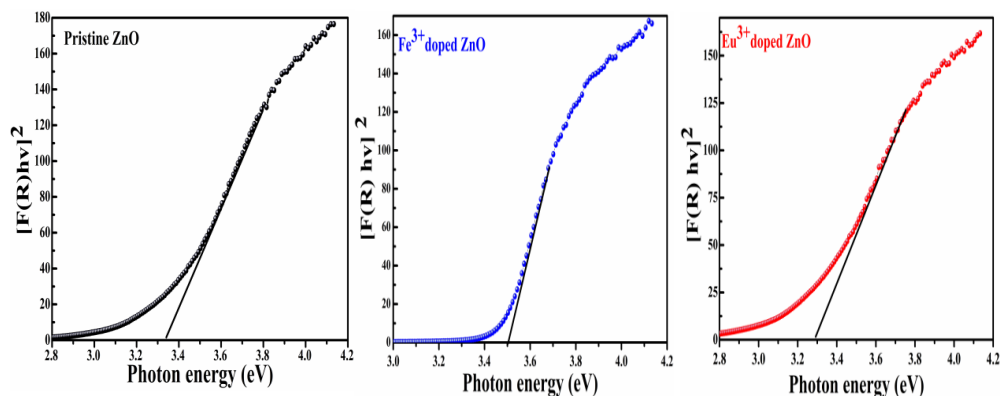*Fig. 4 DRS spectra of pristine, Fe^{3+} and Eu^{3+} doped ZnO NPs*

Fig. 5 Kubelka-Munk plots for pristine, Fe³⁺ and Eu³⁺ doped ZnO NPs

3.5. Magnetic studies

Fig. 6 (a)-(c) depicts the RT magnetization versus applied magnetic field curves for pristine, Fe^{3+} and Eu^{3+} doped ZnO NPs. The pristine ZnO displays the magnetization versus magnetic field curve with a negative slope, confirming the diamagnetism due to the lack of unpaired electrons in thei *d* orbital. The Fe^{3+} doped ZnO NPs displayed the paramagnetic nature at room temperature and may be due to the exchange interaction between the uncoupled Fe^{3+} ions in the ZnO host lattice [13] and may not from the impurity Fe_2O_3 phase, since, Fe_2O_3 is ferromagnetic at room temperature [14]. The Wang et al. [15] noticed the superparamagnetic nature of the Fe doepd ZnO nanoparticles through liquid polyols. Recently, Knanesh et al. [16] reported both ferro and paramagnetism in Fe doped ZnO nanoparticles. Liu et al. [17] also observed the room temperature ferromagnetism in Fe doped ZnO NPs prepared by sol-gel technique. The Eu^{3+} doped ZnO NPs also showed the paramagnetic (PM) behavior. Asper the previous reports, paramagnetsm is an intrinsic nature of Eu^{3+} ions and ferromagnetism is an intrinsic nature of Eu^{2+} ions [18,19]. Yoon et al. [20] observed the weak ferromagnetic behavior in Eu doped ZnO nanoparticles through nanoemulsion process. Tan et al. [21] reported the ferromagnetism in Eu doped ZnO films and could be interpreted by the bound-magnetic-polaron model.
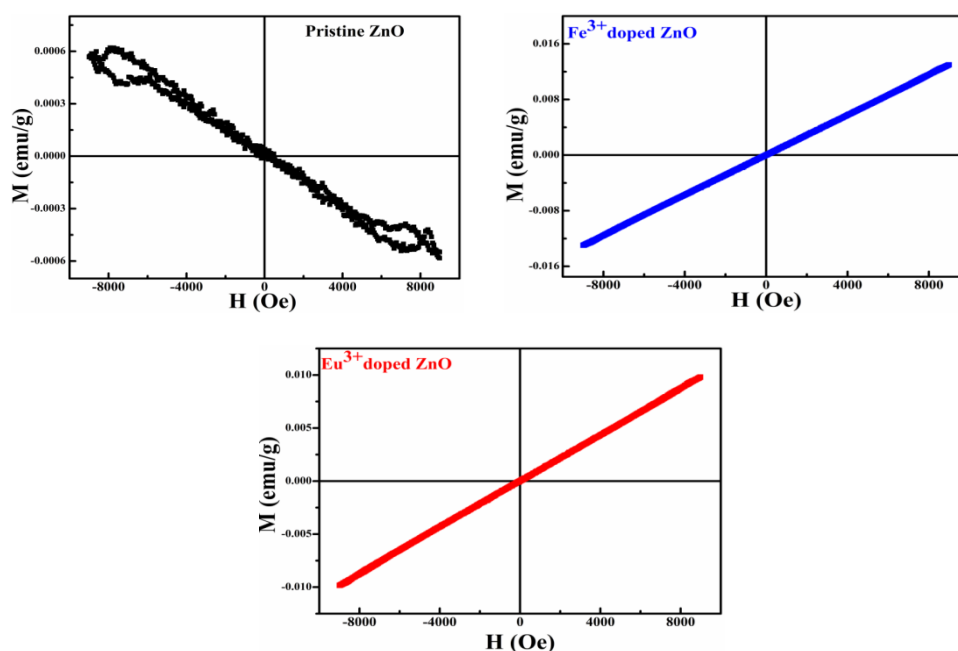

Fig. 6 RT M-H curves for pristine, Fe³⁺ and Eu³⁺ doped ZnO NPs

4. Conclusions

In summary, structural, micro structural, optical and magnetic properties of Pristine, Fe^{3+} and Eu^{3+} doped ZnO NPs fabricated via chemical refluxing route at 100 ^{o}C were investigated. Structural studies revealed that the hexagonal phase with absence of impurities in all the synthesized NPs. TEM studies reveal slightly polydispersed NPs with an irregular size distribution. Room temperature magnetisation studies revealed that the pristine, Fe^{3+} and Eu^{3+} doped ZnO NPs exhibited the dia and paramatic nature.

References

[1] R.R. Galazaka, Inst. Phys. Conf. Ser **43**, 133 (1979).

[2] J.K. Furdyna, J. Appl. Phys. **64**, R29 (1988).

[3] M. Nawrocki, R. Planel, G. Fishman, R.R. Galazaka, Phys. Rev. Lett. **46**, 735 (1981).

[4] J.A. Gaj, R.R. Galazaka, M. Nawrocki, Solid State Commun. **25,** 193 (1978).

[5] A. Mycielski, J. Mycielski, J. Phys. Soc. Jpn. **49**, 809 (1980).

[6] Gunjan Srinet, Ravindra Kumar, Vivek Sajal, J. Appl. Phys. **114**, 033912 (2013).

[7] Gurmeet Singh Lotey, Jaspal Singh, N.K. Verma, Mater. Sci.-Mater. Electron. **24**, 3611 (2013).

[8] Ranjani Viswanatha, Sameer Sapra, Subhra Sen Gupta, B. Satpati, P.V. Satyam, B.N. Dev, D.D. Sarma, Phys. Chem. B, **108**, 6303(2004) .

[9] Atsushi Ishizumi , Satoshi Fujita, Hisao Yanagi, Opt. Mater. **33**, 1116 (2011).

[10] Vijayaprasath Gandhi, Ravi Ganesan, Haja Hameed Abdulrahman Syedahamed, Mahalingam Thaiyan, J. Phys. Chem. C **118**, 9715 (2014) .

[11] J.M. Calleja, Manuel Cardona, Phys. Rev. B **16**, 3753 (1977).

[12] Khan A. Alim, Vladimir A. Fonoberov, Manu Shamsa, Alexander A. Balandin, J. Appl. Phys. **97**, 124313 (2005).

[13] B. Poornaprakash, D. Amaranatha Reddy, G. Murali, R.P. Vijayalakshmi, B.K. Reddy, Physica E **73**, 63 (2015).

[14] B.K. Pandey , A.K. Shahi, Jyoti Shah, R.K. Kotnala, Ram Gopal, Appl. Surf. Sci. **289**, 462 (2014).

[15] Jianwei Wang, Jiaqi Wan, Kezheng Chen, Mater. Lett. **64**, 2373 (2010).

[16] Khanesh Kumar, Mansi Chitkara, Inderjit Singh Sandhu, D. Mehta, Sanjeev Kumar, J. Alloys Compd. **588**, 681(2014).

[17] Huilian Liu, Jinghai Yang, Yongjun Zhang, Lili Yang, MaobinWei, Xue Ding, J. Phys.: Condens. Matter **2**, 145803 (2009).

[18] J. Hite, G.T. Thaler, R. Khanna, C.R. Abernathy, S.J. Pearton, J.H. Park, A.J. Steckl, J.M. Zavada, Appl. Phys. Lett. **89**, 132119 (2006).

[19] M. Hashimoto, A. Yanase, R. Asano, H. Tanaka, H. Bang, K. Akimoto, H. Asahi, Jpn. J. Appl. Phys. **42**, L1112 (2003).

[20] Hayoung Yoon, Jun Hua Wu, Ji Hyun Min, Ji Sung Lee, Jae-Seon Ju, Young Keun Kim, J. Appl. Phys. **111**, 07B523 (2012).

[21] Yongsheng Tan, Zebo Fang, Wei Chen, Pimo He, J. Alloys Compd. **509**, 6321 (2011).